KOOPMAN DECOMPOSITION IN NACA0012 FOIL WAKE

Cesar Monzu Freire, cesar.freire@poli.usp.br
Stergios Pericles Tsiloufas, stergios.tsiloufas@poli.usp.br
Ivan Korkischko, ivan.korkischko@poli.usp.br
Julio R. Meneghini, jmeneg@usp.br
NDF, Department of Mechanical Engineering, POLI, University of São Paulo, CEP 05508-900, São Paulo, SP, Brazil

Davide Bonvini, davide.bonvini@gmail.com
Dipartimento di Ingegneria Meccanica, Facoltà di Ingegneria, Università degli Studi di Padova, via 8 Febbraio 2, 35122 Padova,Italia

Abstract: *The decomposition of the Koopman operator is a new method which can separate a dynamic system in modal components with characteristic frequencies. Stereoscopic particle image velocimetry visualizations and numerical simulation results from two-dimensional spectral/hp element method of the flow past a NACA0012 foil are analyzed using this procedure, along a comparison amongst them. Both numerical and experimental studies are conducted with Reynolds number equal to 5000 and angle of attack 5°. A description of the most energetic modes is presented. The stereoscopic visualizations show a high level of three-dimensional structures, although two-dimensional simulations can lead to very similar results in the case investigated. A discussion of how the three-dimensional structures affect the wake is carried out.*
Keywords: *Dynamic mode decomposition, Particle Image Velocimetry, Coherent Structures*

1. INTRODUCTION

In fluid mechanics, a flow is normally studied using experimental and/or numerical simulations. Even with a great amount of data, sometimes it can be difficult to describe a phenomenon due to its great differences in both spacial and temporal scales. A common strategy is to perform a modal decomposition of the flow in order to point out the most energetic structures that compose it. Hence we are able to separate the scales and neglect many terms of the decomposition without compromising the accurateness of the analysis' results and allowing to make conclusions more easily.

There are many ways of doing such decomposition, including global eigenmodes for linear dynamics, discrete Fourier transforms and Proper Orthogonal Decomposition (POD) for non-linear systems. In the present case, a modal decomposition based on the spectral analysis of the Koopman operator has been employed. Such operator is a linear infinite-dimensional operator that can be associated to any non-linear system. The main advantage of this method is that it does not put any constraint to the characteristics of the flow, which is the case, for example, of the Floquet stability analysis that requires the flow to be periodic in some time interval. Moreover the Koopman operator does not rely on linearization of dynamical equations, therefore it captures the full information of the time evolution of the system.

The flow past an airfoil is the case investigated in this paper. The data was obtained both with numerical simulations using the spectral element method and experimentally using the stereoscopic particle image velocimetry (SPIV) in a circulating water channel at the Fluid-Dynamics Research Group Laboratory (NDF) of the University of Sa?o Paulo (USP). This visualization technique is a evolution of the original particle image velocimetry (PIV) and is able to measure the out of plane velocity, which gives us information about the three-dimensional structures of the flow. The simulations are two-dimensional and the objective of this work is to verify if three-dimensional structures can significantly affect the wake characteristic modes for the case investigated. More information about PIV and SPIV and can be found in Adrian (1991) and Prasad (2000).

This paper is structured as follows. The next section provides basic information about the Koopman operator decomposition. Section 3 gives details about the experimental facilities and the SPIV technique used for the measurements. In section 4 we discuss the numerical simulation implemented to derive a new set of data. Section 5 contains the results obtained with both the experimental and numerical approach while Section 6 is dedicated to the conclusions and the future activities proposed.

2. KOOPMAN OPERATOR DECOMPOSITION

The algorithm used to perform the decomposition of the flow into modes is based on the Koopman operator shown in Rowley et al. (2009). The method is described below.

Let us assume a dynamical system

$$\mathbf{x}_{k+1} = \mathbf{A}\mathbf{x}_k \tag{1}$$

where $\mathbf{A}$ is the so called Koopman operator, an infinite-dimensional linear operator associated with the full nonlinear system dynamics, and $\mathbf{x} \in \mathbb{R}^n$, and n is so large that is impracticable to compute eigenvalues of $\mathbf{A}$ directly. A solution to estimate these eigenvalues is the Krylov method, which takes an initial vector $\mathbf{x}_0$ and the following $m-1$ iterates

to span the Krylov subspace $\{\mathbf{x}_0, \mathbf{A}\mathbf{x}_0, \ldots, \mathbf{A}^{m-1}\mathbf{x}_0\}$. One can project $\mathbf{A}$ onto this m-dimensional subspace and find approximate eigenvectors and eigenvalues of the original operator.

Also, one can write the m-th iterate $\mathbf{x}_m$ as a linear combination of the previous iterates. Generally, we have:

$$\mathbf{x}_m = c_0\mathbf{x}_0 + \ldots + c_{m-1}\mathbf{x}_{m-1} + \mathbf{r} = \mathbf{K}\mathbf{c} + \mathbf{r} \tag{2}$$

where $\mathbf{K}_{n\times m} = [\mathbf{x}_0, \ldots, \mathbf{A}^{m-1}\mathbf{x}_0] = [\mathbf{x}_0, \ldots, \mathbf{x}_{m-1}]$, $\mathbf{c} = (c_0, \ldots, c_{m-1})$ and $\mathbf{r}$ is a residual. We have to chose $\mathbf{c}$ in order to make $\mathbf{r} \perp \text{span}\{\mathbf{x}_0, \ldots, \mathbf{x}_{m-1}\}$, so we can assure that the residual is minimized.

We can show that

$$\mathbf{A}\mathbf{K} = \mathbf{K}\mathbf{C} + \mathbf{r}\mathbf{e}^T \tag{3}$$

where $\mathbf{e} = (0, 0, \ldots, 0, 1) \in \mathbb{R}^m$ and $\mathbf{C}$ is a companion matrix given by

$$\mathbf{C} = \begin{bmatrix} 0 & 0 & \ldots & 0 & c_0 \\ 1 & 0 & & 0 & c_1 \\ 0 & 1 & & 0 & c_2 \\ \vdots & & \ddots & & \vdots \\ 0 & 0 & \ldots & 1 & c_{m-1} \end{bmatrix} \tag{4}$$

One can show that the eigenvalues of $\mathbf{C}$ are a subset of the eigenvalues of $\mathbf{A}$. If $\mathbf{C}\mathbf{a} = \lambda\mathbf{a}$, then $\mathbf{v} = \mathbf{K}\mathbf{a}$ is an eigenvector of $\mathbf{A}$ with eigenvalue λ, i.e.

$$\mathbf{C}\mathbf{a} = \lambda\mathbf{a} \tag{5a}$$

$$\mathbf{K}\mathbf{C}\mathbf{a} = \mathbf{K}\lambda\mathbf{a} \tag{5b}$$

$$\mathbf{A}\mathbf{K}\mathbf{a} = \lambda\mathbf{K}\mathbf{a} \tag{5c}$$

$$\mathbf{A}\mathbf{v} = \lambda\mathbf{v} \tag{5d}$$

Hence if we take m snapshots of the base field $\mathbf{x}_0, \ldots, \mathbf{x}_{m-1}$, one can obtain the Koopman modes $\mathbf{V} = \mathbf{K}\mathbf{T}^{-1}$, where $\mathbf{T}^{-1}$ is the matrix with eigenvectors of $\mathbf{C}$ as columns.

The frequency of each mode is given by

$$f_i = \frac{\arg(\lambda_i)}{2\pi\Delta t} \tag{6}$$

where Δt is the time interval between snapshots.

In this work, the snapshots used as inputs of the method are the two-dimensional $\mathbf{x} = (u, v)$ velocity fields in the numerical case and the three-dimensional $\mathbf{x} = (u, v, w)$ velocity fields for the experimental case. The temporal mean flow was subtracted for each snapshot in order to eliminate the zero-frequency mode in the Koopman decomposition:

$$\mathbf{x}_{\text{mean}} = \frac{1}{m}\sum_{0}^{m}\mathbf{x}_m \tag{7a}$$

$$\mathbf{x}'_m = \mathbf{x}_m - \mathbf{x}_{\text{mean}} \tag{7b}$$

If the system is periodic the Koopman modes are equivalent to the Fourier discrete modes. We can expect from a fully developed flow that nearly all eigenvalues lie on the unit circle, i.e. $|\lambda| = 1$. This indicates that the snapshots $\mathbf{x}_i$ lie on an attracting set.

3. EXPERIMENTAL METHODOLOGY

3.1 Facility and Model Description

The SPIV visualizations were conducted in a circulating water channel facility at the Fluid-Dynamics Research Group Laboratory (NDF) of the University of São Paulo (USP).

The water channel has a $0.70 \times 0.80 \times 7.5m$ test section where the flow velocity can be increased up to $1.0m/s$ with low turbulence level ($< 2\%$). The water channel has glass walls and flor which allows full visualization of the model. More information about the water channel can be found in Ássi et al. (2006).

The NACA0012 model used in the experiments was manufactured by a Dimension rapid prototyping machine and is made of acrylonitrile butadiene styrene (ABS) plastic resin. Three parts with $70mm$ chord and $250mm$ span length were

printed and mounted together in an assembly with $750mm$ span length. The protractor mounted in the top of the model was manufactured by the same method. The protractor was designed to rabbet the model and reduce the assembly error.

Flow-field velocity measurements were made using a stereoscopic particle image velocimetry (SPIV). The water channel was seeded with polyamide particles with average diameter $11\mu m$ which are neutrally buoyant. The particles were illuminated using a Quantel (Brilliant Twins) double cavity pulse Nd-YAG laser that produces a maximum output of $200mJ$ at $532nm$. The horizontal light sheet was imaged using two Imager Pro X 2 Megapixel cameras equipped with Nikon (AF Nikkor $f/1.4D$) lenses of $50mm$ focal length.

3.2 Experimental Procedure

The NACA0012 model was mounted vertically in the water channel, with one end fixed on the bottom of the channel and the other emerged. The cameras were positioned below the water channel in order to record the vortex street formed by the foil. The visualizations were conducted in the middle section of the span. The immersed length was $610mm$.

To avoid reflections problems the foil was kept out of the recording area, as illustrated in figure 1(b). Running visualizations with the model inside the recording area is difficult because of the amount of light reflected by the model, which is much larger than the one reflected by the particles seeded in the flow. Special paints can be used to cover the model in order to chance the wavelength of the reflected light and special lenses can be used to filter the reflected light.

Experiments were conducted with angle of attack $\alpha = 5^{\circ}$ at $\mathrm{Re} = 5000$. The flow velocity in the experiments was kept constant $U_{\infty} = 0.071 \pm 0.003 m/s$. The PIV acquisition frequency was $14.8Hz$ and the number of recorded snapshots were 345 due the capacity of the camera storage, giving a acquisition time of 23 seconds.

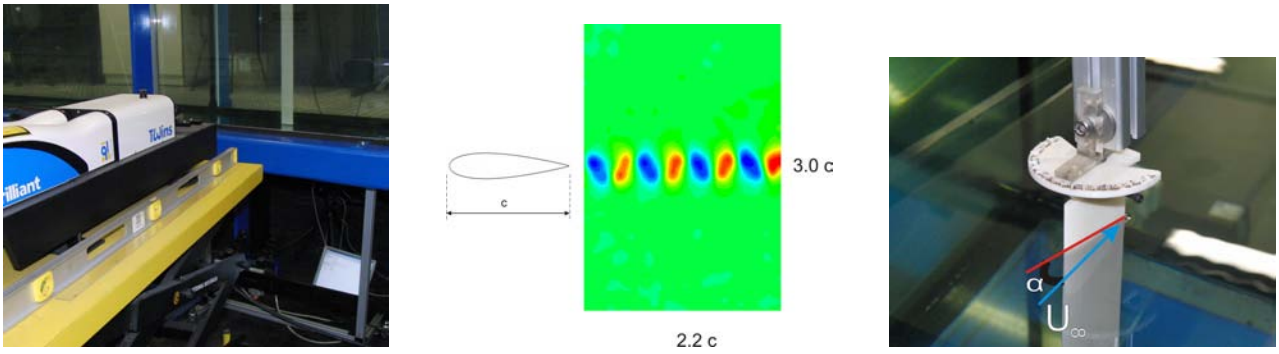

(a) (b) (c)

Figure 1. (a) Experimental setup (b) visualization area (c) model detail

4. SIMULATION METHODOLOGY

In this section we will describe the procedure followed in order to acquire another set of data that describe the evolution of the system. In this case, it was chosen a numeric method which will be described later and, finally, the data obtained was used to make a comparison between this set and the one obtained from the direct measurements in the channel.

Let us assume a fluid with density ρ and dynamic viscosity μ in a uniform flow with velocity U past a two-dimensional NACA0012 airfoil profile with chord c. The numerical evaluation of the problem is based on a spectral/hp element method solver (Karniadakis and Sherwin, 1999) of the incompressible, non-dimensional Navier-Stokes equation, shown in eq. (8).

$$\frac{\partial \mathbf{u}}{\partial t} = -(\mathbf{u} \cdot \nabla)\mathbf{u} - \nabla p + \frac{1}{\mathrm{Re}}\nabla^2 \mathbf{u} \tag{8a}$$

$$\nabla \cdot \mathbf{u} = 0 \tag{8b}$$

where $\mathrm{Re} = U\,c/\nu$ is the non-dimensional Reynolds number and the control parameter of the problem. The kinematic viscosity ν is defined as $\nu = \mu/\rho$.

The Reynolds number taken in consideration was $\mathrm{Re} = 5000$, which is a suitable choice for both numerical and experimental studies available in the laboratory facilities and the angle of attack studied was $\alpha = 5^{\circ}$.

A convergence test was performed in order to define the computational mesh. The upstream length, downstream length, half-width and order of the interpolating polynomial were changed until the mean and RMS values of the forces coefficients C_L and C_D converged with 1% precision. The resulting mesh is shown in Fig. 2. The resulting values were $10c$ for the upstream distance, $50c$ for the lateral sizes, $30c$ for the downstream distance and a 9th order polynomial as shape function in the elements. The upstream and lateral boundary conditions were set as inflow, i.e. unitary velocity in the horizontal direction, the airfoil was set as a viscous wall, i.e. velocity set as zero, and the downstream boundary

condition was set as a outflow, which sets all normal derivatives as zero. The time step for the simulations were chosen to maintain the CFL (Courant-Friedrich-Lewis) number below 1.

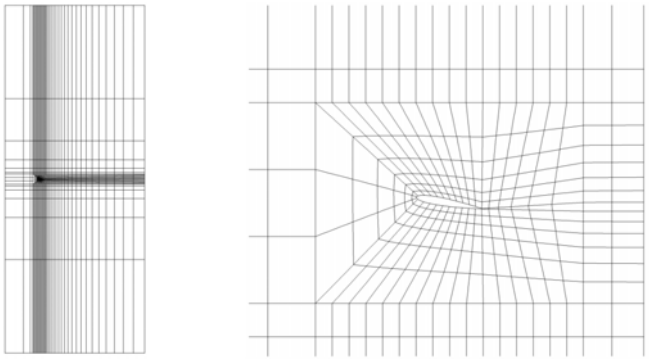

(a) (b)

Figure 2. Resulting mesh. (a) Full computational domain. (b) Airfoil detail.

The initial condition is zero velocity in the computational domain. We ran the simulations for $50s$ in order to assure a fully developed flow. Then, the simulation is restarted and it runs for another $20s$, which is the acquisition period in the experimental study, saving 300 snapshots (velocities fields). These snapshots are the vectors used in the decomposition of the Koopman operator to obtain the characteristic modes of the system.

5. RESULTS

Fig. 3 presents the instantaneous spanwise vorticity field for both numerical and experimental results. The black box in Fig. 3(a) represents the visualization area where the SPIV technique was applied. As we can see in this figure, outside the vortex street there is no significative change in the uniform flow, so the next figures' results are presented inside the red box.

Besides the apparently agreement of the fields, a simple visual analysis of the flow is not enough to compare the results. One important information one has to keep in mind is that the numerical simulations are two-dimensional while the real flow can present three-dimensional characteristics. With the SPIV technique we were able to measure the out of plane component of the fluid velocity in order to study if the flow had a three-dimensional component and its possible effects.

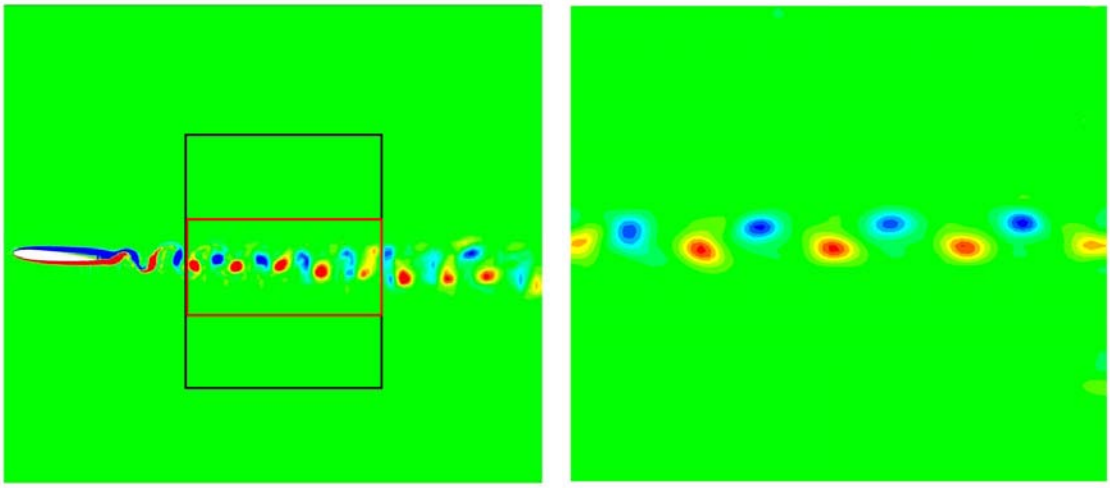

(a) (b)

Figure 3. Instantaneous vorticity field for NACA0012, $\mathrm{Re} = 5000$ and $\alpha = 5^{\circ}$. (a) Numerical result and definition of visualized region (black box) and analyzed region (red box) (b) Full visualized region with SPIV.

Fig. 4 show the non-dimensional w' velocity $w' = \frac{w}{U}$. As we can see the three-dimensional component of the velocity has a significant value, reaching 60% of the far field velocity, and is concentrated in the regions where the spanwise vorticity has its highest values.

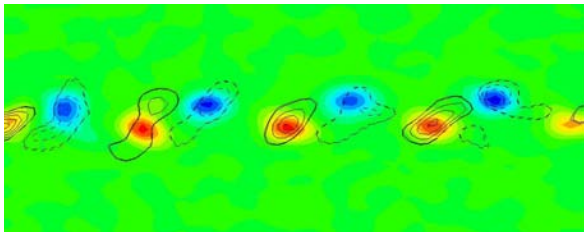

Figure 4. Instantaneous out of the plane velocity: dashed lines represent negative values and the continuous lines the positive ones, V_z/U varies between -0.6 to 0.6. Vorticity contours are indicated by red colour (anticlockwise) and blue colour (clockwise).

One first attempt to analyze the collected data is by looking at how some property evolves in time. For the numerical simulations we were able to calculate the lift force acting on the foil. Fig. 5 illustrates the lift coefficient time series for the fully developed flow and its Fourier transform. The frequency in Fig. 5(b) was indicated as a non-dimensional Strouhal number ($\mathrm{St} = \frac{f\,c}{U}$). One high peak is observed in $\mathrm{St} = 1.85$. A second peak, smaller in amplitude, can be noticed in $\mathrm{St} = 3.70$, a harmonic frequency of the dominant one. Besides the dominant frequency and its harmonic, a small range of frequencies can be found around $\mathrm{St} = 1.0$.

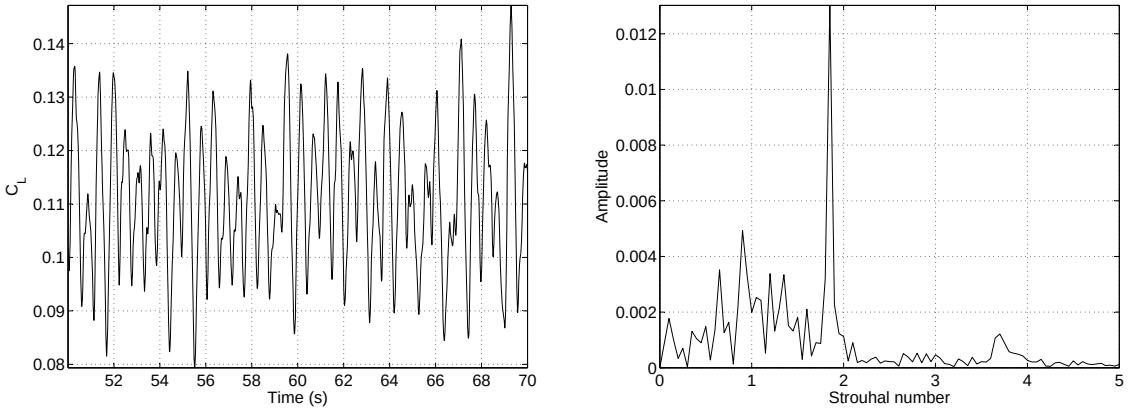

(a) (b)

Figure 5. Numerical results: (a) Temporal signal of lift coefficient. (b) Fourier transform. NACA0012, $\mathrm{Re} = 5000$, $\alpha = 5^{\mathrm{o}}$.

In the experimental procedure no load cell or force transducer were used to measure the lift force because the foil was fixed in the bottom of the water channel and the friction force between the glass floor and the model should be considered. If the inferior tip of the model was not fixed, the foil would present a bending mode of vibration, just like a flutter movement that would affect the entire flow. To study the time and frequency responses in the experimental case the transverse velocity v was measured in a point inside the vortex street. Fig. 6 shows the transverse velocity time series and its Fourier transform.

In comparison with the numerical case a good agreement can be found in the value of the dominant frequency. For the experimental case $\mathrm{St}_{exp} = 1.91 \pm 0.08$ while for the numerical case $\mathrm{St}_{num} = 1.85 \pm 0.05$. In Fig. 6(b) there is no other significant frequency besides vortex shedding frequency and its harmonic. One has to keep in mind that the numerical result consider an integral quantity such as the lift coefficient while the experimental result considers only a local property. The frequencies captured around $\mathrm{St} = 1.0$ observed in Fig. 5 probably come from the flow around the foil that affects the lift force.

Applying the Koopman decomposition on both numerical and experimental velocity fields we can obtain the dynamic modes, the eigenvalues of the Koopman operator and the spectrum of frequency of these modes. Fig. 7 presents the first and second modes for the experimental and numerical simulations considering the in-line velocity u. Fig. 8 shows the same results for the transversal velocity v and Fig. 9 illustrate the modes for the out of plane velocity w for experimental measurements.

As we can see, the experimental and numerical first mode are very similar for both in-line u and transverse velocity v. The second mode also shows a good global agreement, but some local differences, mainly for the transverse velocity v.

Fig. 10(a) and Fig. 11(a) illustrates the eigenvalues of the Koopman operator for the experimental and numerical case,

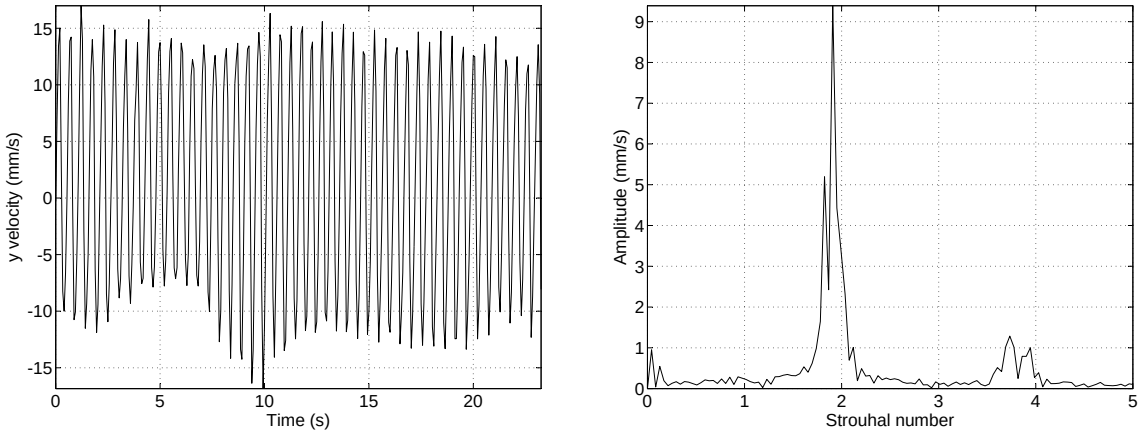

(a) (b)

Figure 6. Experimental results: (a) Temporal signal of transversal velocity. (b) Fourier transform. NACA0012, $\mathrm{Re} = 5000$, $\alpha = 5^{\mathrm{o}}$.

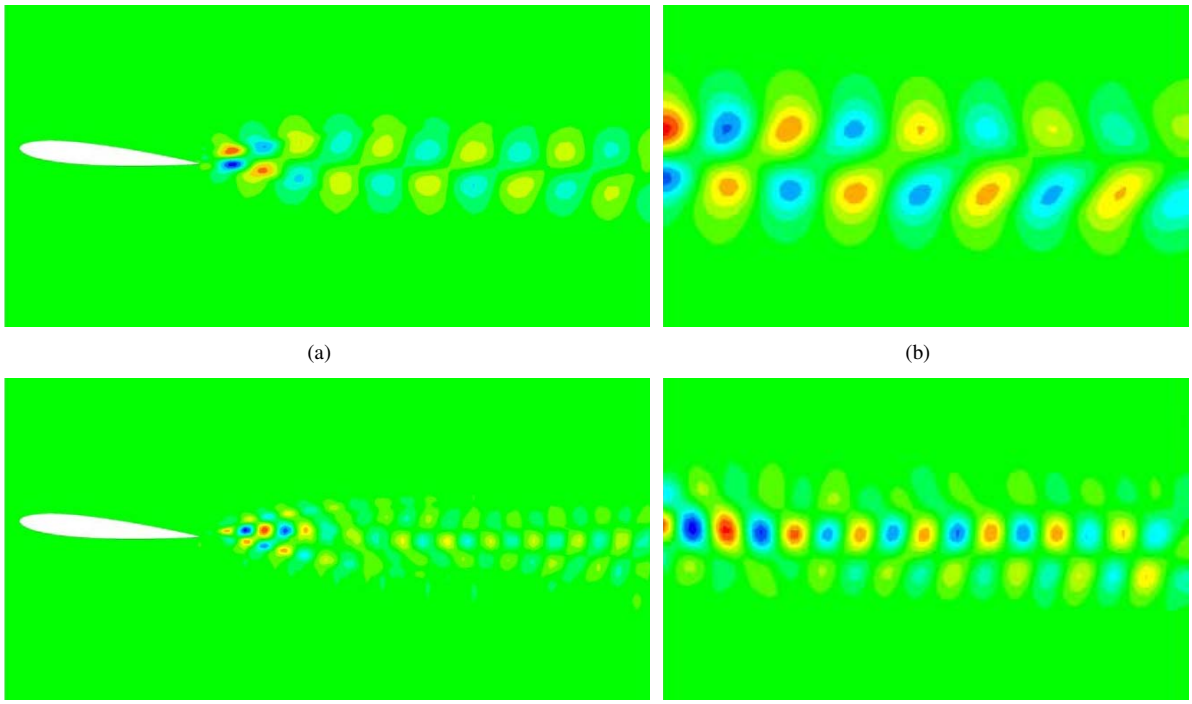

(a) (b)

(c) (d)

Figure 7. Contours of u velocity. Numerical results: (a) First mode (c) Second mode; Experimental results: (b) First mode (d) Second mode. NACA0012, $\mathrm{Re} = 5000$, $\alpha = 5^{\mathrm{o}}$.

respectively. We can see that most of the eigenvalues of the operator lies in the unity circle, which shows that the flow is fully developed in both cases. The energy of each mode is shown in Fig. 10(b) for the experimental mode and in Fig. 11(b) for the numerical modes.

The spectrum of frequencies for both cases are very similar to the ones obtained by the Fourier transform of the C_L and velocity signals. It is interesting to compare both spectrums for the numerical case. In Fig. 5(b) the amplitude in the region around $\mathrm{St} = 1.0$ is higher than the amplitude of the second harmonic frequency in $\mathrm{St} = 3.7$. In the other hand, for the spectrum of frequency of the Koopman modes, the relative vector norm for the second mode is higher than the vector norm in the region close to $\mathrm{St} = 1.0$. That means that the second mode has less energy than the phenomenon that occurs in $\mathrm{St} = 1.0$, but this phenomenon does not consist in a mode and the small structures found in that region have less energy than the second mode.

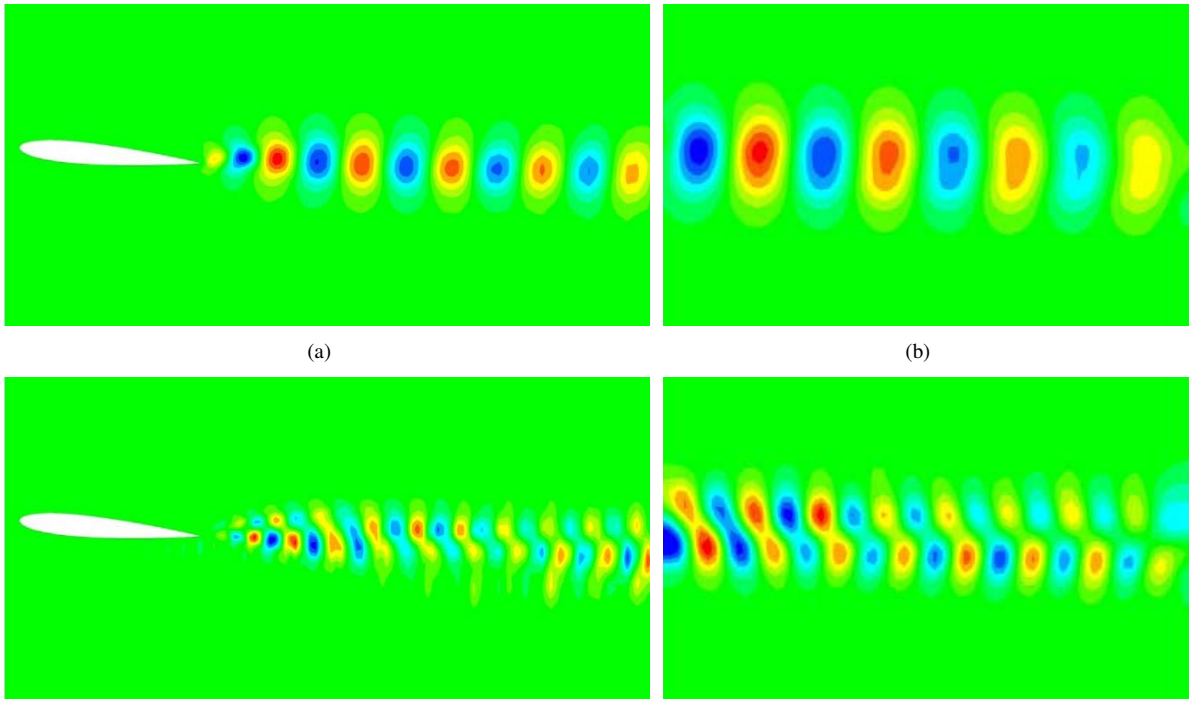

(a) (b)

(c) (d)

Figure 8. Contours of v velocity. Numerical results: (a) First mode (c) Second mode; Experimental results: (b) First mode (d) Second mode. NACA0012, $\mathrm{Re} = 5000$, $\alpha = 5^{\mathrm{o}}$.

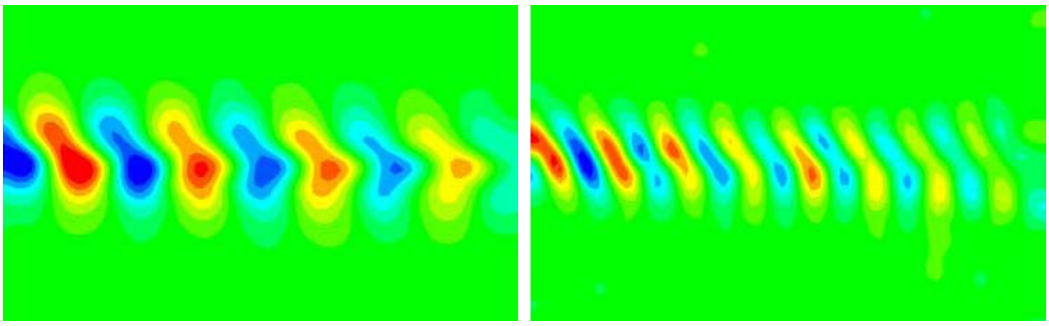

(a) (b)

Figure 9. Contours of w velocity. Experimental results: (a) First mode (b) Second mode. NACA0012, $\mathrm{Re} = 5000$, $\alpha = 5^{\mathrm{o}}$.

6. CONCLUSION AND FUTURE ACTIVITIES

One of the goals of this work was to verify if three-dimensional structures can change significantly the wake pattern in this given condition. Analyzing the SPIV results, one can clearly notice that the spanwise velocity component is not negligible, reaching 60% of the far field velocity. However, comparing the three-dimensional experimental measures with two-dimensional numerical results, there is no change in the vortex shedding frequency or in the modes topology.

The dynamic mode decomposition of the Koopman operator is a powerful method able to separate the structures of the flow according to its frequencies. Both in numerical and experimental cases the method was capable of extracting the most energetic mode with good accuracy, when comparing to a Fourier transform of a temporal variable such as the lift coefficient for the numerical case or the v velocity of a wake point in the experimental case.

This work was the first part of an ongoing research. Further activities consists on new experiments with different visualizations setups and new numerical simulations.

Some objectives are to visualize the flow in the spanwise direction and to introduce the model inside the SPIV visualization area.

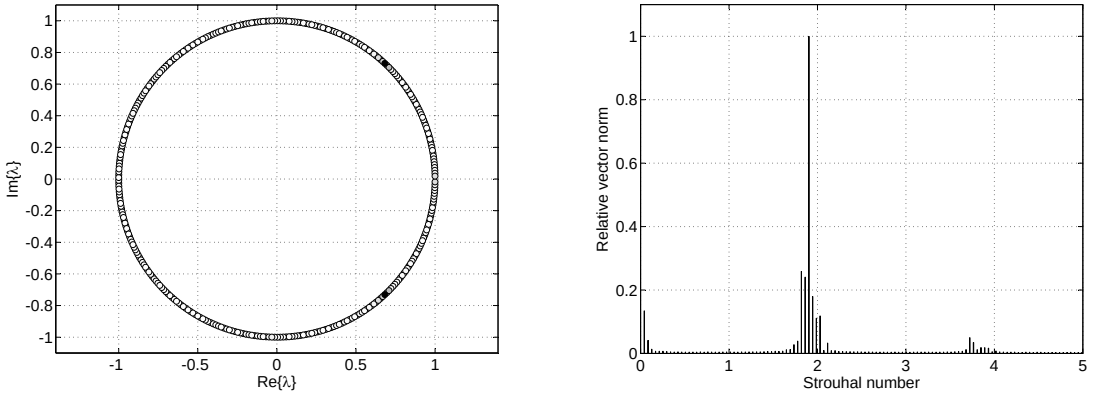

(a) (b)

Figure 10. Experimental results: (a) Eigenvalues of the Koopman operator. Coloring goes from white (least energetic) to black (most energetic). (b) Spectrum of frequencies. NACA0012, $\mathrm{Re} = 5000$, $\alpha = 5^{\mathrm{o}}$.

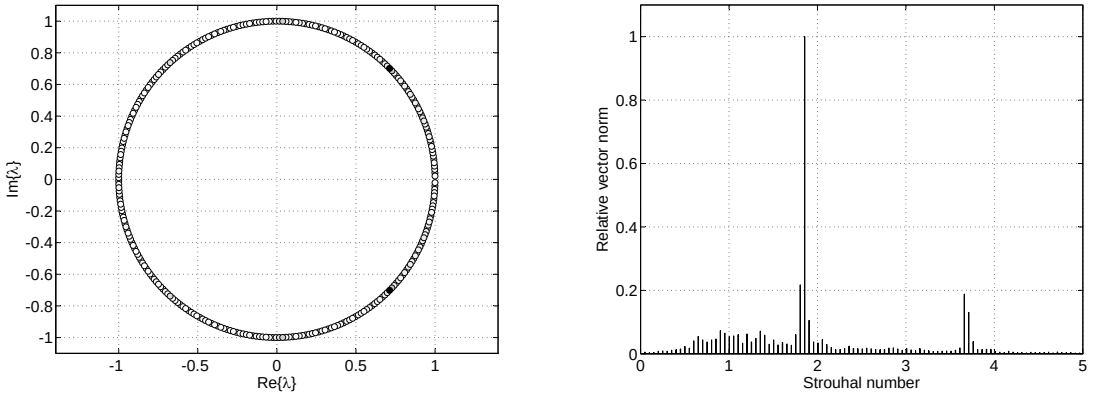

(a) (b)

Figure 11. Numerical results: (a) Eigenvalues of the Koopman operator. Coloring goes from white (least energetic) to black (most energetic). (b) Spectrum of frequencies. NACA0012, $\mathrm{Re} = 5000$, $\alpha = 5^{\mathrm{o}}$.

7. ACKNOWLEDGEMENTS

We would like to acknowledge the financial support provided by Fapesp, CNPq, and Embraer. All the computing resources were provided by NDF - University of So Paulo.

8. REFERENCES

A K. Prasad, 2000, "Stereoscopic particle image velocimetry". Experiments in Fluids, Vol. 29, pp. 103–116.

Ronald J. Adrian, 1991, "Particle-imaging techniques for experimental gluid mechanics". Annual Review of Fluid Mechanics, Vol. 23, pp. 261–304.

G. E. Karniadakis and S. J. Sherwin, "Spectral/hp element methods for computational fluid dynamics". 2nd. ed. Oxford University Press, 1999.

C.W. Rowley, I. Mezic, S. Bagheri, P. Schlatter and D.S. Henningson, 2009, "Spectral analysis of nonlinear flows". Journal of Fluid Mechanics, Vol. 641, pp. 115–127.

G.Ássi, 2005, "Estudo esperimental do efeito de interferência no escoamento ao redor de cilindros alinhados". Dissertação de Mestrado. Escola Politécnica, USP.

G. R. S. Ássi, J. R. Meneghini , J. A. P. Aranha , P. W. Bearman , E. Casaprima, 2006, "Experimental investigation of flow-induced vibration interference between two circular cylinders". Journal of Fluids and Structures, Vol. 22, pp. 819–827.

9. RESPONSIBILITY NOTICE

The author(s) is (are) the only responsible for the printed material included in this paper.